كلية الهندسة بشبرا
FACULTY OF ENGINEERING AT SHOUBRA
ERJ
PRINT ISSN 3009-6049
ONLINE ISSN 3009-6022

ENGINEERING RESEARCH JOURNAL (ERJ)
Volume (53) Issue (2)
April 2024, pp:68-81
https://erjsh.journals.ekb.eg

Study of The Thermal Performance Characteristics of Shell and Semi-circular Tube Heat Exchanger Using Both Baffles and Nanofluid

N.M. Almulla[1], M.A. Moawed[1], M.A. Abd-Elrahman[1] , Mohamed R. Salem*[1]

[1] Department of Mechanical Engineering, Faculty of Engineering at Shoubra, Benha University, Cairo, Egypt
* Corresponding Author.
E-mail: : mohamed.abdelhamid@feng.bu.edu.eg , me_mohamedreda@yahoo.com

Abstract : This study investigates the performance characteristics of a shell-tube heat exchanger using three techniques to improve heat transfer rate: baffles, nanofluids, and semicircular tubes (SCTs). The experiments are done using six heat exchangers of SCTs with different base spacing ratios (β), alumina/water nanofluid loaded on the shell side with different nanoparticle loadings (φ), and single-segmental baffles mounted with cut ratio ($\delta = 16.5\%$), and pitch ratio ($\lambda = 1.47$). The results show that when SCTs are used instead of CCTs, the heat transfer coefficient and friction factor are greater, and they increase when the SCT spacing ratio increases. The $\overline{Nu}_{sh}$ and f_{sh} of nanofluids are greater than the base fluid at the same flow condition, and they grow as φ increases. Besides, the inclusion of nanoparticles in water on the shell side has a greater influence on these increases with SCTs than CCTs. The hydrothermal performance index (HTPI) is evaluated using the Stanton number of the shell side and f_{sh} ratios. The maximum obtained HTPI is 3.19 for a shell-SCT heat exchanger with baffles of δ=16.5%, λ=1.47, alumina/water nanofluid concentration of φ=1.5%, and SCTs of β=55.1%. Finally, correlations are provided to predict $\overline{Nu}_{sh}$, f_{sh}, and the HTPI of the tested heat exchangers.

Keywords: Heat exchanger; Baffles; Semi-circular tube; γ-Al_2O_3/water nanofluid; Heat transfer augmentation.

1. INTRODUCTION

Improving heat exchange efficiency significantly impacts cost, material, and energy savings. Shell and tube heat exchangers are widely used in various industries, including chemical plants, refineries, aerospace, defense, and maritime. They can eliminate process heat, preheat feed water, and cool hydraulic and lubricating oils [1-4]. Therefore, active and passive methods were suggested to increase their heat exchange rate [5-9]. Baffles are passive techniques that direct flow and serve four essential functions: supporting tubes, increasing turbulence, removing dead spots, and reducing temperature differences. Available in impermeable or perforated shapes [10-12].

Moreover, high-performance cooling and heating operations face thermal conductivity restrictions, limiting heat transfer gmentation techniques. Nanotechnology can address this issue by using small solid particles with high thermal conductivities, increasing thermal conductivities [13-15]. Nanofluids are fluids with solid nanoparticles smaller than 100 nm in size, typically less than 4% in particle volume [13]. Liquid molecules mix with particles, creating layered structures like solids. A thin, aligned layer of liquid molecules transfers heat from the solid to the liquid next to it. To improve thermal conductivity, a thermal bridge is created between solid nanoparticles and bulk liquid [14-20], as depicted in Fig. 1. Nanofluids with various particle volume concentrations (φ) can be created to investigate pressure drop and heat transfer properties. The φ of the suspended nanoparticles is defined as follows [21]:

$$\varphi = \frac{V_{np}}{V_{total}} = \left[\frac{V_{np}}{V_{np}+V_{bf}}\right] = \left[\frac{(m_{np}/\rho_{np})}{(m_{np}/\rho_{np})+(m_{bf}/\rho_{bf})}\right] \quad (1)$$

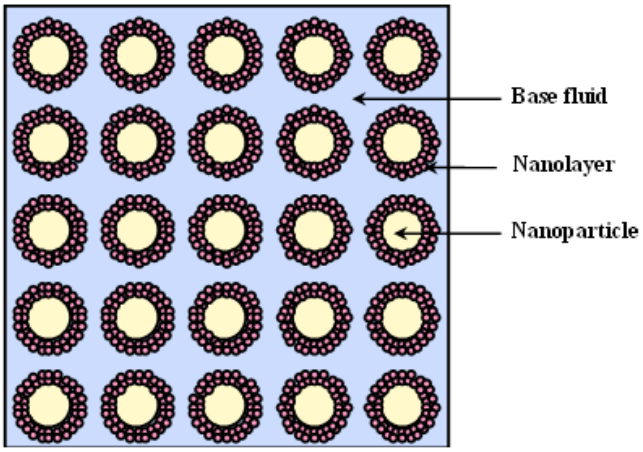

Fig. 1: Representation of nanofluid structure [20].

Numerous studies have examined the impact of baffle geometry on heat exchanger performance attributes. Additionally, studies have explored the integration of nanoparticle mixtures in base fluids as passive heat transfer enhancement mediums. This section provides an overview of prior research on the combined effect of baffles and nanofluid insertion. Magalhães et al. [22] developed a Python differential transient model for a shell-and-tube heat exchanger, determining fluid temperature profiles, heat transfer coefficient, and heat load. Jahangiri et al. [23] studied alumina nanoparticles' impact on microchannel water flow, finding decreased outlet temperature, increased vortices strength, and increased heat transfer rate. Khetib et al. [24] studied the impact of nanofluid, baffles, Reynolds numbers, tube configurations, and geometrical parameters on heat transfer rate, finding triangular form 2.1% more efficient than a rectangle. Larger baffles led to increased pressure loss. Bahiraei et al. [25] studied the irreversibility characteristics of a shell and tube heat exchanger with a helical baffle. They used boehmite nanofluid and water, finding platelet nanoparticles producing maximum thermal entropy and oblate spheroid particles having minimal irreversibility. Alazwari and Safaei [26] investigated the thermal performance and flow parameters of a shell and tube heat exchanger using distilled water and hybrid nanofluid. They found that a 135° baffle angle maximized heat evacuation and improved thermal performance.

Sharifat et al. [27] simulated the effects of tube pass ratio, twisted helical baffle, and Al_2O_3/water nanofluid on heat transfer in shell-and-tube heat exchangers. They found that Reynolds number and tube pass ratio increased heat transfer, while baffle space reduced the friction factor. Silva [28] compared heat exchanger baffle geometry and graphene-based nanofluids, finding 0.025% wt. graphene as optimal performance fluid. Gugulothu and Sanke [29] simulated heat exchanger performance using 22% cut segmental and helical baffles, finding higher heat transfer coefficients and performance indexes for 40° helical baffles with Al_2O_3/water nanofluid. Yang et al. [30] studied helical baffles' impact on hydrothermal aspects and irreversibility behavior in water-CuO nanofluid turbulent forced convection flow. Results showed increased Nusselt number with Re and nanoparticle concentration, while pressure drop decreased with baffle pitch. Akcay and Akdag [31] studied CuO-water nanofluid's hydrothermal performance in circular ducts with varying baffle angles, finding significant thermal increase with the largest enhancement factor and relative friction factor at 90° and 150° baffle angles. Souayeh et al. [32] studied baffle and dimple turbulator effects on heat transfer and pressure drop in Fe_3O_4 magnetic nanofluid, finding increased Nusselt numbers at lower magnetic field strengths. Rana et al. [33] studied CuO nanofluid thermal-hydraulic characteristics in a microscale step channel, finding increased volume fraction, Reynolds number, Nusselt number, and 164% improved heat transfer with a baffle, but at higher pumping power requirements. Bouselsal et al. [34] Ma enhanced tube/shell heat exchanger efficiency with nanoparticles and Al_2O_3-MWCNT hybrid nanofluid, improving heat transmission by 103.1%.

The literature review shows that studies on the dual effect of baffles and nanofluids are limited compared to independent analysis. Most studies were done numerically, and no laboratory investigations have been conducted concurrently. Furthermore, research shows that combined baffles and nanofluids improve hydrothermal performance compared to individual use. Besides, these studies used CCTs as a heat transfer surface area, although several studies [35-38] indicated that SCTs give greater heat transfer rates. Therefore, this work investigates the hydrothermal attributes of a shell-tube heat exchanger with a counter-flow configuration, including CCTs or SCTs as heat transfer surfaces. It also covers the flow of cooling γ-Al_2O_3/water nanofluid loaded with nanoparticle volume concentrations ($0 \leq \varphi \leq 1.5\%$) on the shell side. In addition, single segmental baffles with a constant cut ratio of $\delta = 16.5\%$ and pitch ratio of $\lambda = 1.47$ are considered.

2 Experimental apparatus

This study uses hot and cold loops in equipment, with the hot circuit consisting of a heating cabinet, pump, valves, and connecting pipes. The cold circuit consists of a cooling system, pump, valves, shell, flow meter, and connecting pipes. The current setup and test section are depicted in Figs. 2 & 3. The heating and cooling units used 100-liter stainless steel tanks; each tank is housed within a galvanized steel tank with a 20mm gap, insulated with polyurethane spray foam. Four 5 kW electric heaters are fixed in the heating cabinet to heat water to the required temperature. The cooling cabinet contains two cooling units with a combined capacity of 20.5

kW, removing heat from water or nanofluid. These units operate in series/parallel to prevent thermal overloads. Each cabinet has four ports, two are for the bypass line and heat exchanger, and two are drain exit points. Two 3-hp centrifugal pumps with a maximum flow rate of 110 l/min are used. Pump-1 pumped heating water out of the tank, measured by flow meter-1, and returned to the heating tank. Pump-2 transferred cooling water circulated through the heat exchanger's shell and returned to the cooling tank. The experiment setup utilized polyvinyl chloride and flexible nylon tubing for connections, with stainless steel T-shaped connectors for the differential pressure transducer and shell main line.

Six shell-tube heat exchangers with a counter-flow configuration are built using various geometrical parameters. These heat exchangers have 14 SCTs or 7 CCTs, with copper tubes measuring 1250 mm in length and 12.7 and 11.5 mm in outer and inner diameters. They are arranged with a 25 mm spacing from center to center. Each SCT is formed by cutting off a CCT with a plasma cutting tool, followed by longitudinally soldering a sheet with the same material, length, diameter, and thickness. Protuberances from welding processes are carefully removed.

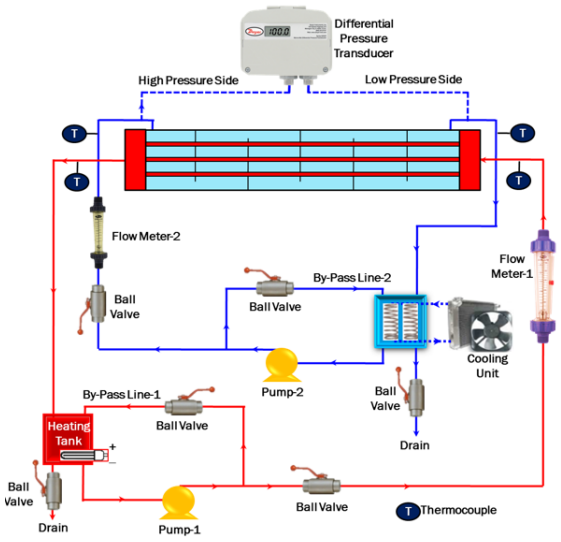

Fig. 2: Schematic representation of the present apparatus.

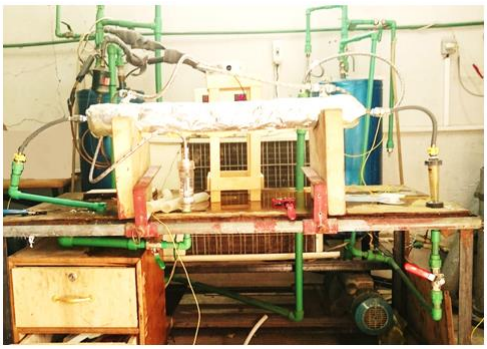

Fig. 3: Photo of the present experimental setup.

Mild steel is used to construct heat exchangers' shells, which are rolled into a cylindrical shape. Two flanges are welded on the shell ends, which are bolted to headers. The apparatus contains two galvanized steel headers to supply/receive water to/from tubes. They are tanks with 2mm walls and inner diameter, and length of 101.6mm and 120mm, respectively. Twelve circular galvanized steel housing dies (Fig. 4) have a 3mm wall thickness with holes like heat exchanger tubes. Drilling is done using a laser-cut machine. Besides, three rubber gaskets are incorporated to prevent leaks between the header nipple and blind flange and between the housing die and shell nipple. They are connected via dies, sealing potential gaps between tubes and die holes. A copper sheet with a 0.6-mm thickness creates baffles, which are cut and drilled using the laser. They are soldered to tubes using copper welding. Fig. 5 displays schematic diagrams, while Table 1 lists the key parameters of utilized heat exchangers and nanoparticle concentrations. The key variables of the geometrical parameters are defined according to Eqs. (2-4). Besides, the shell has welded-on inlet and exit ports with constant cross sections, 30mm from the neighbouring end. Its outer surface is thermally isolated with ceramic fibre, asbestos rope, and glass wool insulation. Two calibrated flow meters (±5% reading accuracy) are used to measure the volume flow rates of main loop fluids. Flow meter-1 measures 10 to 100 l/min for the hot fluid loop, while meter-2 measures 1.8 to 18 l/min for the cold fluid line. Besides, four calibrated K-type thermocouples measure the inlet and exit temperatures of shell and tube fluids inserted 50mm from heat exchanger ports and are displayed on a digital thermometer with a ±0.1°C resolution. Additionally, a calibrated digital differential pressure transducer measures shell-side pressure with a ±1% accuracy and a working range of 0-103.4 kPa.

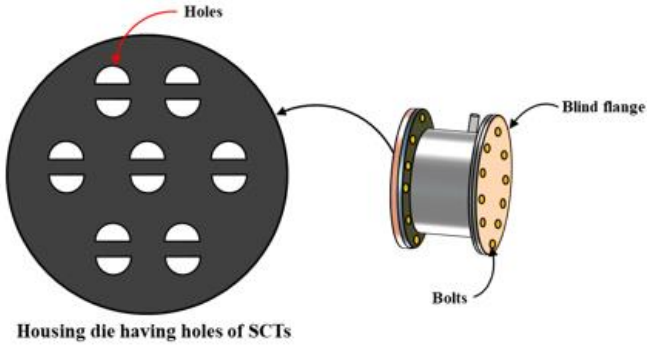

Fig. 4: The header of the heating water.

Table 1: Key parameters of utilized heat exchangers and nanoparticle concentrations.

#Runs	S_b (mm)	β	φ	δ	p_b (mm)	N_b	λ
18	CCT		0	No baffles			
36			0.5%				
54			1.0%				
72			1.5%				
90	3	23.6%	0				
108			0.5%				
126			1.0%				
144			1.5%				
162	5	39.4%	0				
180			0.5%				
198			1.0%				
216			1.5%				
234	7	55.1%	0				
252			0.5%				
270			1.0%				
288			1.5%				
306	CCT		0	16.5%	150	8	1.47
324			0.5%				
342			1.0%				
360			1.5%				
378	7	55.1%	0				
396			0.5%				
414			1.0%				
432			1.5%				

$$\beta = \frac{S_b}{d_{t,o}} \quad (2)$$

$$\delta = \frac{A_{Edge\ cut}}{A_{Baffle}} \quad (3)$$

$$\lambda = \frac{p_{Baffle}}{d_{Baffle}} \quad (4)$$

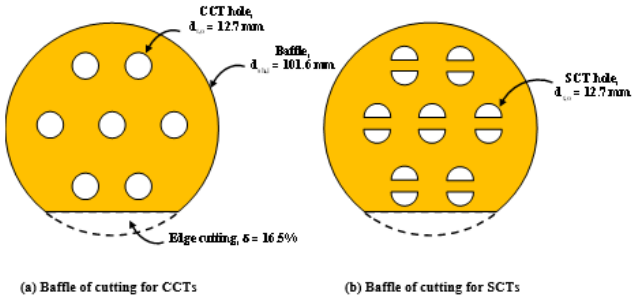

Fig. 5: Key characteristics of the baffles utilized in the present work.

3.Nanofluid preparation

Nanofluids are used as heat transfer working fluids by preparing a stable suspension of gamma-alumina (γ–Al_2O_3) nanoparticles with 99.99% purity, 30 nm particle size, and 220 m^2/g surface area. The thermophysical characteristics of these particles are listed in Table 2. This study prepared γ–Al_2O_3/water nanofluid with three different particle volume concentrations of 0.5, 1, and 1.5%. Dispersion is achieved by mixing the required volume in a measuring flask, and the mixture is ultrasonically vibrated for 8 hours to ensure uniform dispersion. The agitator bath is used for two consecutive days to achieve stable suspension. Besides, nanoparticles settle slowly after the first 6 days of static nanofluid conditions, but complete settlement occurs after 14 days. It should be noted that before each run, the prepared Al_2O_3/water nanofluid is circulated for an hour to prevent sedimentation. After 1.5% concentration experiments, Al_2O_3/water nanofluid is diluted with water to lower concentrations, and an agitator and ultrasonic vibrator are used for loading new nanoparticles.

Table 2: Properties of γ–Al_2O_3 nanoparticles.

Thermal conductivity ($W/m.°C$)	Density (kg/m^3)	Specific heat ($J/kg.°C$)
36	3600	773

4.Experimental procedures

The experiments start with attaching thermocouples to the inlet and outlet of shell and tube sides and assembling a shell-tube heat exchanger, heating and cooling units, pumps, piping, flow meters, thermocouples, and a differential pressure transducer. Data is collected by filling heating and cooling tanks with water from the domestic water supply. nanofluids are prepared with the required concentration of nanoparticles and poured into the cooling tank. The heater, cooler, and pumps are turned on. γ–Al_2O_3/water nanofluid is diluted with water to reach a lower concentration, and an agitator and an ultrasonic vibrator are used for each new nanoparticle loading. In total, 432 experiments are conducted on the six heat exchangers. The steady-state condition is started when thermocouple readings show a maximum variation of 0.5°C within 20 minutes and is achieved when stable fluid inlet and outlet temperatures are done, with a 0.1°C variation in the minutes before the test. Table 3 provides the operational condition range.

Table 3: Range of fluid operating conditions

Parameters	Range or value
Shell-side flow rate, l/min	8.1–18.4 ($3550 \leq Re_{sh} \leq 14580$)
Shell-side inlet temperature, ℃	15, 20, 25 ($3.13 \leq Pr_{sh} \leq 7.28$)
Nanoparticles volume concentration, %	0, 0.5, 1, 1.5
Tube-side flow rate, l/min	42.7
Tube-side inlet temperature, ℃	60

5 Calculation methodology

In the present analysis, the thermophysical properties of the cooling and heating fluids in the shell and the tubes are calculated at the mean temperatures, $T_{sh,m}$ and $T_{t,m}$, respectively.

$$T_{sh,ave} = (T_{sh,i} + T_{sh,o})/2 \quad (5)$$

$$T_{t,m} = (T_{t,i} + T_{t,o})/2 \quad (6)$$

For γ–Al_2O_3/water nanofluid, the thermophysical properties are determined using Eqs. (7-17) [39-43].

$$k_{nf} = k_{static} + k_{Brownian} \quad \textbf{(7)}$$

$$k_{static} = k_{bf}\left[\frac{k_{np} + 2k_{bf} + 2\varphi(k_{np} - k_{bf})}{k_{np} + 2k_{bf} - \varphi(k_{np} - k_{bf})}\right] \quad \textbf{(8)}$$

$$k_{Brownian} = 5 * 10^4\, \Gamma\, \chi\, \varphi\, \rho_{bf}\, Cp_{bf} \sqrt{\frac{\kappa\, T}{\rho_{np}\, d_{np}}} \quad \textbf{(9)}$$

$$\Gamma = (1722.3\varphi - 134.63) - (6.04\varphi - 0.4705)T \quad \textbf{(10)}$$

$$\chi = 0.0017(100\varphi)^{-0.0841} \quad \textbf{(11)}$$

$$\mu_{nf} = \mu_{static} + \mu_{Brownian} \quad \textbf{(12)}$$

$$\mu_{static} = \frac{\mu_{bf}}{[1-\varphi]^{2.5}} \quad \textbf{(13)}$$

$$\mu_{Brownian} = 5 * 10^4\, \Gamma\, \chi\, \varphi\, \rho_{bf} \sqrt{\frac{\kappa\, T}{\rho_{np}\, d_{np}}} \quad \textbf{(14)}$$

$$\rho_{nf} = \varphi\rho_{np} + (1-\varphi)\rho_{bf} \quad \textbf{(15)}$$

$$Cp_{nf} = \frac{\varphi(\rho_{np}Cp_{np}) + (1-\varphi)(\rho_{bf}Cp_{bf})}{\rho_{nf}} \quad \textbf{(16)}$$

$$Pr_{nf} = \frac{\mu_{nf}\, Cp_{nf}}{k_{nf}} \quad \textbf{(17)}$$

The heat transfer rates (Q_{sh} and Q_t) on the shell and tube sides are calculated using Eqs. (18) and (19). Theoretically, the two loads are equal ($Q_t = Q_{sh}$), while there is a difference between them to some extent. Therefore, the average rate, Q_{ave}, is addressed. For all tests, compared to the average load, the difference between the two rates does not fluctuate by more than ±4.8%. Besides, the overall thermal conductance is estimated via Eq. (22):

$$Q_{sh} = \dot{m}_{sh} Cp_{sh}(T_{sh,o} - T_{sh,i}) \quad (18)$$

$$Q_t = \dot{m}_t Cp_t(T_{t,i} - T_{t,o}) \quad (19)$$

$$Q_{ave} = \frac{|Q_t| + |Q_{sh}|}{2} \quad (20)$$

$$\Delta Q_{ave}(\%) = \frac{|Q_t| - |Q_{sh}|}{Q_{ave}} * 100 \quad (21)$$

$$U_i A_{t,i} = \frac{Q_{ave}}{\Delta T_{L.M}} \quad (22)$$

$$\Delta T_{L.M} = \frac{(\Delta T_i - \Delta T_o)}{\ln\left[\frac{\Delta T_i}{\Delta T_o}\right]} = \frac{(T_{t,i} - T_{sh,o}) - (T_{t,o} - T_{sh,i})}{\ln\left[\frac{T_{t,i} - T_{sh,o}}{T_{t,o} - T_{sh,i}}\right]} \quad (23)$$

$$A_{t,i} = 7\pi d_{t,i} L_t \quad \text{For CCTs} \quad (24)$$

$$A_{t,i} = 14 d_{t,i} L_t (0.5\pi + 1) \quad \text{For SCTs} \quad (25)$$

$$\overline{Nu}_t = 0.023 * Re_t^{0.8} * Pr_t^{0.4} \quad (26)$$

$$\overline{h}_t = \frac{\overline{Nu}_t . k_t}{d_{t,h}} \quad (27)$$

$$d_{t,h} = d_{t,i} \quad \text{For CCTs} \quad (28)$$

$$d_{t,h} = \frac{\pi d_{t,i}}{\pi + 2} \quad \text{For SCTs} \quad (29)$$

$$\frac{1}{U_i A_{t,i}} = \frac{1}{\overline{h}_{sh} A_{t,o}} + \frac{1}{\overline{h}_t A_{t,i}} \quad (30)$$

$$\overline{Nu}_{sh} = \frac{\overline{h}_{sh}\, d_{sh,h}}{k_{sh}} \quad (31)$$

$$d_{sh,h} = \frac{d_{sh,i}^2 - 7d_{t,o}^2}{d_{sh,i} + 7d_{t,o}} \quad \text{For CCTs} \quad (32)$$

$$d_{sh,h} = \frac{\pi\, d_{sh,i}^2 - 7\pi\, d_{t,o}^2}{\pi\, d_{sh,i} + 7 d_{t,o}(\pi + 2)} \quad \text{For SCTs} \quad (33)$$

$$Re_t = \frac{4\dot{m}_{t,tube}}{\pi d_{t,h} \mu_t} \quad (34)$$

$$Re_{sh} = \frac{4\dot{m}_{sh}}{\pi d_{sh,h} \mu_{sh}} \quad (35)$$

$$St_{sh} = \frac{\overline{Nu}_{sh}}{Re_{sh}.\, Pr_{sh}} \quad (36)$$

$$f_{sh} = \frac{\Delta P_{sh}\, d_{sh,h}}{2 L_{sh}\, \rho_{sh} u_{sh}^2} = \frac{\Delta P_{sh}\, \pi^2\, \rho_{sh}\, d_{sh,h}^5}{32\, L_{sh}\, \dot{m}_{sh}^2} \quad (37)$$

6 Uncertainty analysis

The approach developed by Kline and McClintock [44] is applied to evaluate the uncertainty of all parameters. The uncertainties of key parameters are summarized in Table 4.

Table 4: Maximum uncertainties in the main parameters.

Parameter	**Uncertainty (%)**
Tube-side Reynolds number	±1.70
Sell-side Reynolds number	±2.10
Tube-side average Nusselt number	±1.40
Tube-side average heat transfer coefficient	±1.41
Sell-side average Nusselt number	±2.70

Shell-side average heat transfer coefficient	±2.96
Overall heat transfer coefficient	±2.24
Shell-side Fanning friction factor	±6.70
Shell-side Stanton number	±3.67
Hydrothermal performance index	±6.10

7 Apparatus validation and data verification

Validating heat transfer coefficients and friction factors involves tracking flow/temperature measurements on the shell side and comparing them to known correlations. $\overline{Nu}_{sh}$ for water flow through the shell is compared to Gnielinski [45], Eq. (38), and $\overline{Nu}_{sh}$ for turbulent flow. Fanning friction factor is evaluated using Filonenko's correlation [46], Eq. (39), and f_{sh} results are compared. The validation process is conducted for shell and CCTs, with working requirements summarized in Table 5. Comparisons showed consistent results for $\overline{Nu}_{sh}$ and f_{sh} determinations, with maximum variances of 7.8% and 5.5%, ensuring precision in experimental tools and measurement techniques.

$$\overline{Nu}_{sh} = \frac{\frac{f_{sh}}{2}(Re_{sh} - 1000)Pr_{sh}}{1 + 12.7\sqrt{\frac{f_{sh}}{2}}\left(Pr_{sh}^{2/3} - 1\right)}\left[1 + \left(\frac{d_{sh,h}}{L_{sh}}\right)^{2/3}\right] \quad (38)$$

$$f_{sh} = 0.25(1.82\log Re_{sh} - 1.64)^{-2} \quad (39)$$

Table 5: Validation working specifications.

Parameter	Range or Value
Tube-side water flow rate, l/min	42.7 ($Re_t \approx 23070$)
Tube-side inlet temperature, ℃	60 ($Pr_t \approx 3.05$)
Shell-side water flow rate, l/min	8.1–18.4 ($3550 \leq Re_{sh} \leq 9760$)
Shell-side inlet temperature, ℃	15, 20, 25 ($5.52 \leq Pr_{sh} \leq 7.28$)

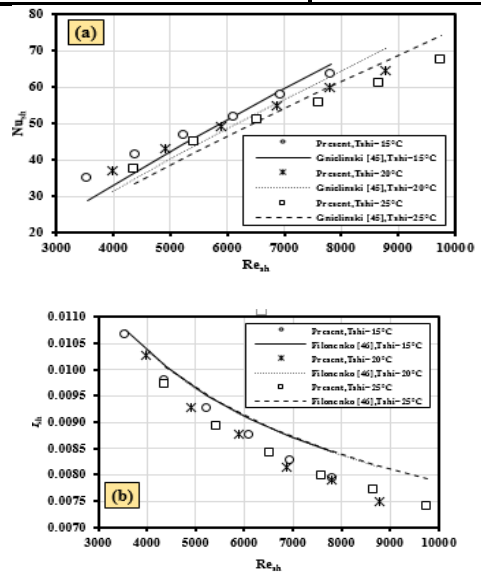

Fig. 6: Findings of the validation runs: (a) $\overline{Nu}_{sh}$, (b) f_{sh}.

8 Results and discussions

8.1 Plain heat exchanger with nanofluid at different nanoparticle concentrations

In this analysis, four heat exchangers; one with CCTs and the other three with SCTs are subjected to 288 experimental tests. The SCTs have bases that are 3 or 5 or 7 mm apart. Thus, the base spacing ratios are 23.6%, 39.3%, and 55.1%, respectively. In these tests, γ-Al_2O_3 nanoparticle loadings of 0, 0.5%, 1.0%, and 1.5% by volume are all considered. The operating settings for the heating water in the tube side are held constant at 60°C inlet temperature and a total flow rate of 42.7 l/min, while the operating conditions for the cooling nanofluid are changed in line with Table 3. Fig. 7 demonstrates the documented results for $\overline{\mathrm{Nu}}_{\mathrm{sh}}$ and f_{sh} owing to incorporating the alumina nanoparticles on the shell side at β = 55.1% and $T_{\mathrm{sh,i}}$ = 20°C as a sample of the findings. Fig. 8 shows the consistent results due to incorporating SCTs with different spacings at φ = 0% and $T_{\mathrm{sh,i}}$ = 15°C as a sample of the findings. Also, Fig. 9 shows the documented results for $\overline{\mathrm{Nu}}_{\mathrm{sh}}$ in addition to f_{sh} by altering the shell-side operating circumstances at β = 39.3% and φ = 0% as a sample of the outputs.

Fig. 7 shows that the $\overline{\mathrm{Nu}}_{\mathrm{sh}}$ of nanofluids is greater than the base fluid's at the same flow condition and that this improvement grows as φ increases even at constant $\mathrm{Re}_{\mathrm{sh}}$ and $\mathrm{T}_{\mathrm{sh,i}}$. The average increase in $\overline{\mathrm{Nu}}_{\mathrm{sh}}$ at the same shell side flow rate is 15.4%, 31.3%, and 48.5% at φ = 0.5%, 1.0%, and 1.5%, respectively. This demonstrates that the poor heat transfer performance of base fluid (water) may be addressed by increasing heat transfer rates using nanofluids as a thermal-fluid medium. In addition to the increased thermal conductivity of nanofluids, the interactions, micro-convection, and Brownian motion of nanoparticles, as well as the ensuing disruption of the boundary layer, may be to blame for the increased heat transfer coefficients of nanofluids that have been observed. Besides, the f_{sh} of nanofluids is also higher than that of the base fluid at the same flow state, and this increase grows as φ increases even at the same $\mathrm{Re}_{\mathrm{sh}}$. For φ = 0.5%, 1.0%, and 1.5%, respectively, the average increase in f_{sh} at the same shell side flow rate is 6.5%, 16.5%, and 25.8%. This can be traced back to the high viscosity of the nanofluid, which rises as the amount of nanoparticles in the base fluid increases.

Additionally, Fig. 8 displays comparable findings as a result of dividing the internal tubes at various base spacing ratios. $\overline{\mathrm{Nu}}_{\mathrm{sh}}$ and f_{sh} are higher when SCTs are incorporated than when CCTs are. There are various causes for this, one of which is expanding the SCTs' contact area rather than the CCTs' (from $(\pi d_{t,o}L_t)$ for CCT to be $(\pi d_{t,o}L_t + 2d_{t,o}L_t)$ for pair of SCTs). Moreover, as shown in Eqs. (32) and (33), dividing

the internal tubes results in a smaller shell-side hydraulic diameter, which increases the Reynolds number for the same shell-side flow rate and changes the flow behaviour. Besides, the $\overline{\mathrm{Nu}}_{\mathrm{sh}}$ and f_{sh} increase with increasing the SCT spacing ratio. This can be attributed to increasing the flow turbulence level around the tubes by increasing the SCT spacing ratio. This breaks the thermal and velocity boundary layers of the shell-side flow, which increases the flow mixing and consequently increases both the heat transfer rate and shell-side flow resistance. At the smallest spacing ratio between the SCTs (β = 23.6%), the flow velocity beside their bases is very small where the SCTs block the flow at this region, while this is accompanied by a larger spacing between the tube's outer surfaces, which reduces the overall pressure drop. Moreover, the $\overline{\mathrm{Nu}}_{\mathrm{sh}}$ and f_{sh} rise when the SCT spacing ratio rises. This is explained by the fact that as the SCT spacing ratio is increased, the flow turbulence level around the tubes increases. This causes the thermal and velocity boundary layers of the shell-side flow to be broken. As a result, the heat transfer rate and shell-side flow pressure drop are increased. The flow rate adjacent to the SCTs' bases is very low where they obstruct the flow at this location at the shortest spacing ratio between the SCTs (β = 23.6%) however this is followed by a wider spacing between the tube's outer surfaces, which lowers the overall pressure drop. On the other hand, expanding the SCTs' spacing enables a greater flow of cooling water on the shell's side between their bases. Moreover, the spaces between the exterior surfaces of the tubes are kept to a minimum. As a result, the flow mixing and turbulence levels around the tube surfaces rise, increasing the heat transfer rate as well as the flow pressure loss on the shell side. Compared with employing CCTS, the average increases in the $\overline{\mathrm{Nu}}_{\mathrm{sh}}$ are 48%, 63.3%, 80.5% at β = 23.6%, 39.4%, and 55.1%, respectively. The associated increases in the f_{sh} are 1.7%, 9.3%, and 19.5%, respectively. From Fig. 9, it is clear from all runs that $\overline{\mathrm{Nu}}_{\mathrm{sh}}$ is reduced at the same $\mathrm{Re}_{\mathrm{sh}}$ as the inlet temperature of the shell-fluid flow rises. This is explained by the fact that when the water or nanofluid temperature rises, the Prandtl number falls. In addition, it is clear that $\mathrm{T}_{\mathrm{sh,i}}$ have a negligible impact on f_{sh}. This can be attributed to the lower effect of viscosity variation compared with the inertia force. Additionally, Fig. 9 makes it clear that raising $\mathrm{Re}_{\mathrm{sh}}$ augments $\overline{\mathrm{Nu}}_{\mathrm{sh}}$. This is supported by raising the Reynolds number, which raises the level of fluctuations and causes fluid layers to mix around internal tubes. On the other hand, as $\mathrm{Re}_{\mathrm{sh}}$ increases, f_{sh} decreases, supporting the idea that momentum forces overcome viscous forces.

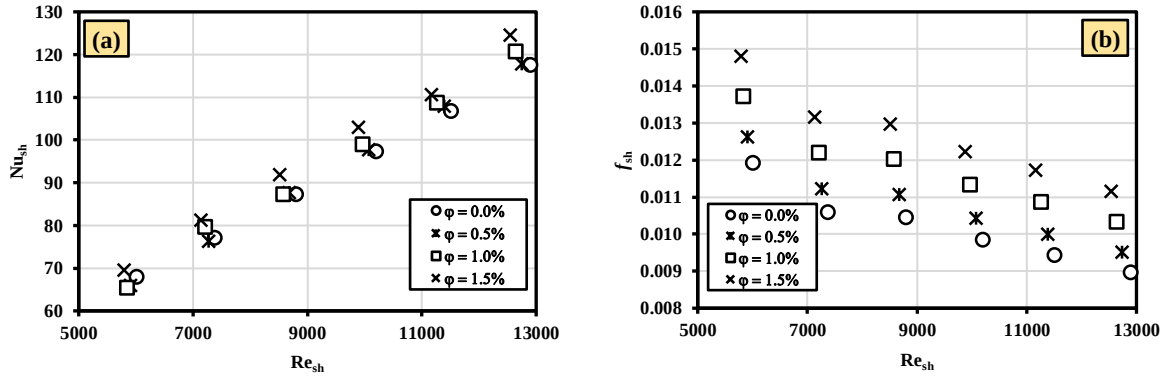

Fig. 7: Performance parameters of examined heat exchangers vs. shell-Reynolds number at different alumina nanoparticle loadings (β = 55.1%, $T_{sh,i}$ = 20°C); (a) $\overline{Nu}_{sh}$, (b) f_{sh}.

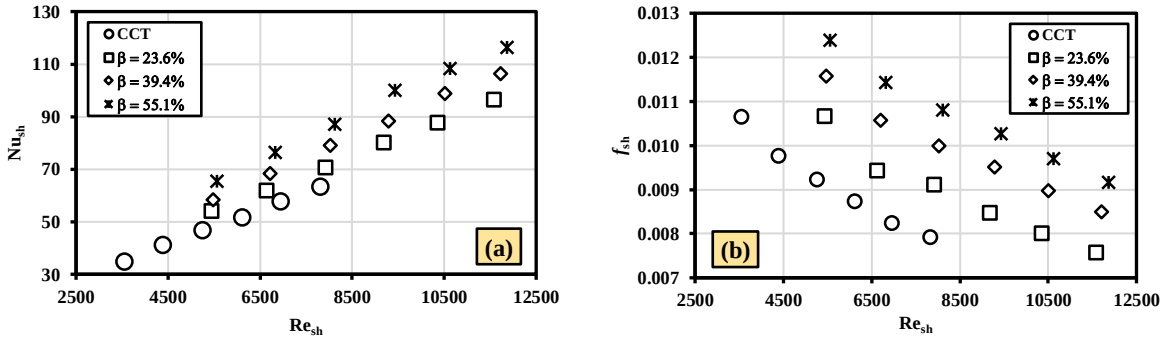

Fig. 8: Performance parameters of examined heat exchangers vs. shell-Reynolds number at different base spacing ratios (φ = 0%, $T_{sh,i}$ = 15°C); (a) $\overline{Nu}_{sh}$, (b) f_{sh}.

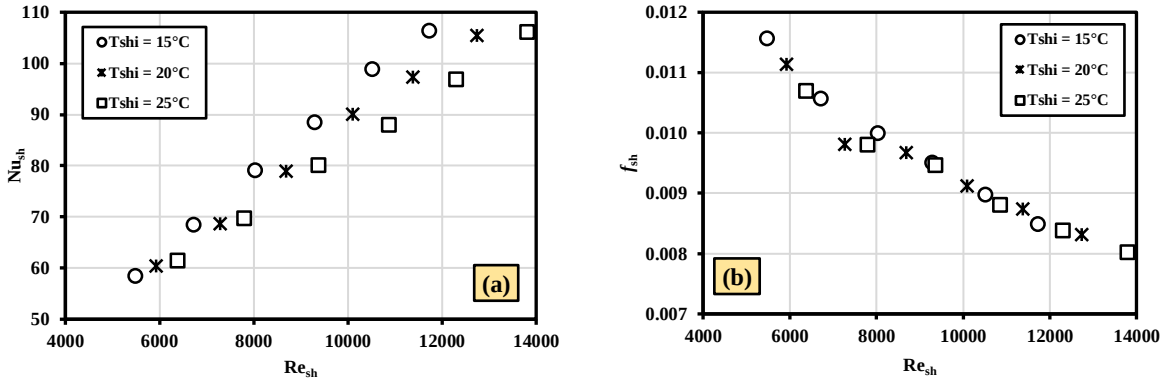

Fig. 9: Performance parameters of examined heat exchangers vs. shell-Reynolds number at different shell-side operating conditions (φ = 0%, β = 39.3%); (a) $\overline{Nu}_{sh}$, (b) f_{sh}.

8.2 Heat exchanger with baffles and γ-Al_2O_3/water nanofluid at different nanoparticle concentrations

In this investigation, two heat exchangers with baffles and alumina/water nanofluid in the shell are subjected to 144 experimental tests. CCTs or SCTs with a base spacing of 7 mm (β = 55.1%) are used in the experiments. There are also 8 single segmental baffles (pitch of 150 mm; λ = 1.47) with a cutting ratio of δ = 16.5%. The shell side contains cold water or γ-Al_2O_3/water nanofluid with nanoparticle concentrations ranging from 0.5% to 1.5%. The operating conditions for the heating water in the tube side are kept constant at 60°C inlet temperature and a total flow rate of 42.7 l/min, whereas the operating conditions for the cooling γ-Al_2O_3/water nanofluid are adjusted as shown in Table 3. Fig. 10 shows the documented findings for $\overline{\mathrm{Nu}}_{\mathrm{sh}}$ and f_{sh} due to the γ-Al_2O_3 nanoparticle inclusion on the shell side at $T_{sh,i}$ = 15°C as a sample of the results. It is demonstrated that the $\overline{\mathrm{Nu}}_{\mathrm{sh}}$ of nanofluids is higher than the base fluid's at the same shell flow condition and that this improvement grows as increases even at constant $\mathrm{Re}_{\mathrm{sh}}$ and $\mathrm{T}_{\mathrm{sh,i}}$. The average increase in $\overline{\mathrm{Nu}}_{\mathrm{sh}}$ at the same shell side flow rate is 11.4%, 16.8%, and 20.6% at φ = 0.5%, φ = 1.0%, and φ = 1.5%, respectively, with the use of CCTs. While the equivalent gains are, respectively, 22.1%, 25.4%, and 31.6% when incorporating SCTs (β = 55.1%).

This text highlights the potential benefits of using nanofluids as a thermal-fluid medium, which can lead to increased heat transfer rates and improved performance compared to base fluid (water). Furthermore, it is shown that the f_{sh} of nanofluids is greater than that of the base fluid under the same flow circumstances and that this increase develops as φ increases even when the $\mathrm{Re}_{\mathrm{sh}}$ remains constant. When CCTs are used, the average increase in f_{sh} at the same shell side flow condition is 9.6%, 12.0%, and 15.5% for φ = 0.5%, φ = 1.0%, and φ = 1.5%, respectively. With integrating SCTs (β = 55.1%), the equivalent increases in f_{sh} are 15.6%, 18.3%, and 22.1%, respectively. This can be attributed to the nanofluid's high viscosity, which increases as the proportion of γ-Al_2O_3 nanoparticles in the cooling water grows. Besides, Fig. 10 shows that the increases in $\overline{\mathrm{Nu}}_{\mathrm{sh}}$ and f_{sh} by the inclusion of γ-Al_2O_3 nanoparticles in the water on the shell side have a greater influence on the increases with SCTs than CCTs. This is supported by increasing the contact area of the tubes as well as the smaller shell-side hydraulic diameter by dividing the internal tubes, which increases the Reynolds number for the same shell-side flow rate and changes the flow behavior. This raises the turbulence level of the shell-side flow, enhancing both the Brownian motion of the nanoparticles and the resulting micro-convection heat transfer. Consequently, this improves total heat transmission while increasing shell-side pressure loss.

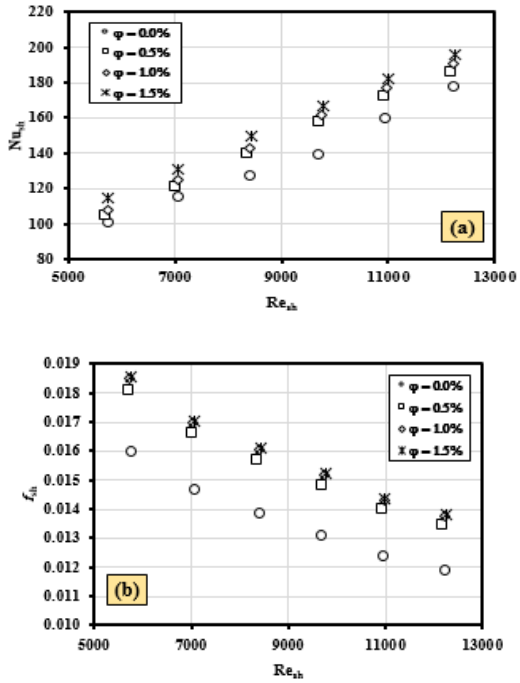

Fig. 10: Performance parameters of examined heat exchangers vs. shell-Reynolds number at different alumina loadings (β = 55.1%, δ = 16.5%, λ = 1.47, $T_{sh,i}$ = 15°C); (a) $\overline{Nu}_{sh}$, (b) $\boldsymbol{f_{sh}}$.

8.3 Hydrothermal performance index

To be considered a successful heat exchange technique, the increase in heat transfer generated by SCTs, nanofluid, and/or baffles should be greater than the corresponding increase in fluid pumping power. This study evaluates the hydrothermal performance index (HTPI) using St_{sh} and f_{sh} ratios [47,48] calculated using SCTs/γ–Al_2O_3/water nanofluid/baffles and CCTs as heat transfer surfaces, as follows:

$$HTPI = \frac{St_{sh,m}/St_{sh,0}}{(f_{sh,m}/f_{sh,0})^{1/3}} \quad \textbf{(40)}$$

In Eq. (40), $St_{sh,m}$ and $f_{sh,m}$ represent the modified Stanton number and Fanning friction factor, respectively, for heat exchangers with SCTs, γ-Al_2O_3/water nanofluid, and/or baffles. Furthermore, $St_{sh,0}$ and $f_{sh,0}$ represent their corresponding values at the same shell side flow rate and temperature, without baffles and with CCTs and base fluid (water). Fig. 11 shows the average HTPI value for all runs with different parameters. This explanation aims to clarify the significance of the equation in relation to monitoring heat transfer and flow resistance in heat exchangers by engaging the proposed tested techniques. Fig. 11a illustrates that raising the SCTs base spacing ratio increases the HTPI, and this increase is grown by increasing the Al_2O_3 nanoparticle lading. In the absence of baffles, the average HTPI is 1.17 and 1.35 when CCTs are replaced with SCTs of β = 23.6% and 55.1%, respectively, at nanoparticle concentrations of φ = 0. With nanoparticle loading of φ = 1.5, the corresponding average HTPI increases to 1.64 and 1.87, respectively. Furthermore, at φ = 0, when CCTs are replaced with SCTs with base spacing ratios of 23.6% and 55.1%, the average HTPI is 1.74 and 2.09, respectively, at a cut ratio of δ = 16.5%. Besides, Fig. 11b depicts the average HTPI versus γ-Al_2O_3 nanoparticle concentration using a plain heat exchanger (no baffles). The HTPI is clearly more than one for all operating settings and increases with increasing nanoparticle loading on the shell side. When CCTs and SCTs (β = 55.1%) are used, the average HTPI value is 1.14 and 1.43 at φ = 0.5, respectively. Furthermore, with φ = 1.5, the corresponding average HTPI rises to 1.4 and 1.87. Furthermore, Fig. 11c displays the average HTPI of the evaluated heat exchangers with baffles of δ = 16.5%, λ = 1.47, and various γ-Al_2O_3 nanoparticle loadings on the shell side. It is also obvious that raising the concentration of nanoparticles boosts HTPI. When CCTs and SCTs (β = 55.1%) are used, the average HTPI value at φ = 0.5 is 1.79 and 2.74, respectively. Furthermore, when φ = 1.5, the average HTPI increases to 1.9 and 2.93. As well, Fig. 11d displays the HTPI of the tested heat exchanger in which their shell is engaged with baffles of δ = 16.5%, λ = 1.47, γ-Al_2O_3/water nanofluid of nanoparticle concentration of φ = 1.5, and SCTs of β = 55.1%. Increasing the cooling medium flow rate and/or intake temperature reduces the HTPI. The HTPI is 3.19 and 3.06 at $T_{sh,i}$ = 15°C and 25°C, respectively, at the lowest shell-side flow rate (8.1 l/min). When the shell-side flow rate is increased to 18.4 l/min, the HTPI drops to 2.84 and 2.8 at $T_{sh,i}$ = 15°C and 25°C, respectively.

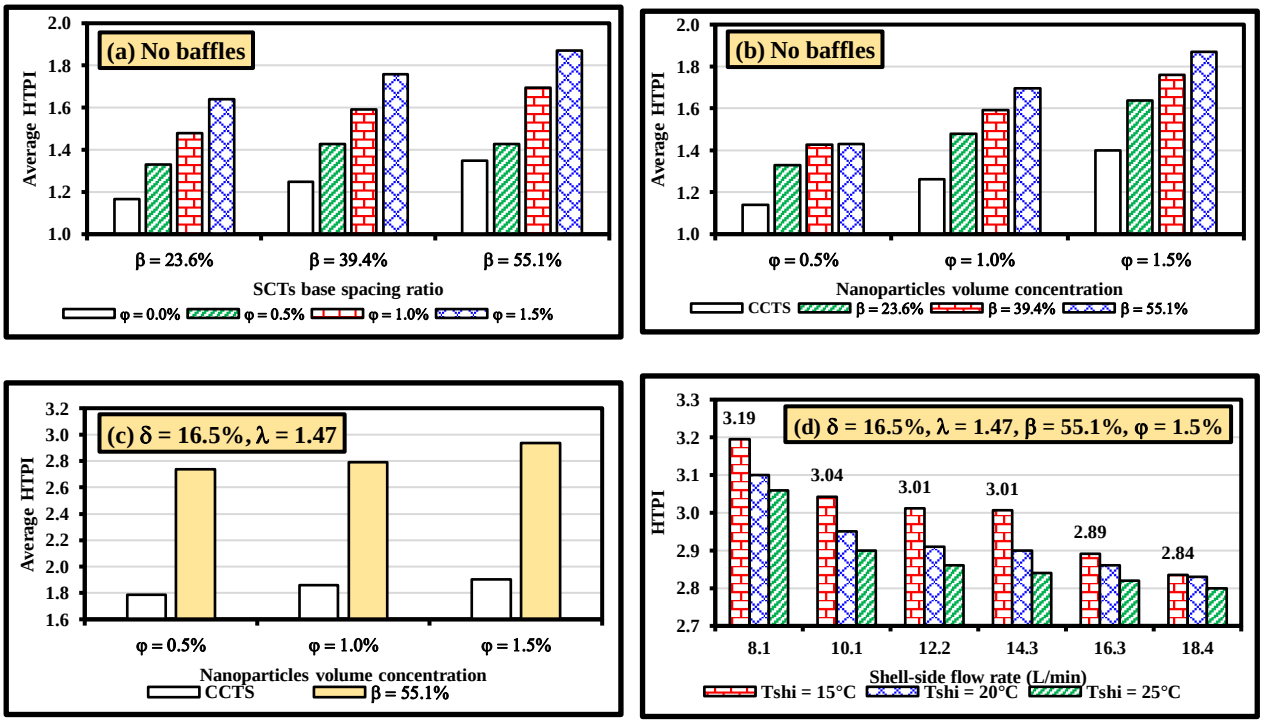

Fig. 11: The HTPI of the examined heat exchangers at different design conditions.

9 Correlations

Using the recorded data, correlations are provided to predict the $\overline{\mathrm{Nu}}_{\mathrm{sh}}$ and f_{sh} of the shell-side, as well as the HTPI of the tested heat exchangers for water or γ-Al_2O_3/water nanofluid with nanoparticle concentrations less than 1.5% passing through the shell side of a counter flow shell and tube heat exchanger having CCTs or SCTs with base spacing ratios ranging from 23.6% to 55.1%

For plain heat exchangers (without baffles):

$$\overline{Nu}_{sh} = 0.0437\ Re_{sh}^{0.7016}\ Pr_{sh}^{0.5103}\ (1+\varphi)^{16.8004}\ (1+\beta)^{0.8465} \quad (41)$$

$$f_{sh} = 0.246\ Re_{sh}^{-0.3868}\ (1+\varphi)^{13.4503}\ (1+\beta)^{0.7753} \quad (42)$$

$$HTPI = 1.1187\ Re_{sh}^{-0.0248}\ Pr_{sh}^{-0.0683}\ (1+\varphi)^{23.4919}\ (1+\beta)^{0.7095} \quad (43)$$

Eqs. (41-43) are valid for shell-side Reynolds and Prandtl numbers from 3550 to 13900 and from 3.34 to 7.28, respectively.

For heat exchangers with single segmental baffles:

$$\overline{Nu}_{sh} = 0.096\ Re_{sh}^{0.6773}\ Pr_{sh}^{0.4756}\ (1+\varphi)^{5.5012}\ (1+\beta)^{1.1056} \quad (44)$$

$$f_{sh} = 0.3156\ Re_{sh}^{-0.3784}\ (1+\varphi)^{1.4256}\ (1+\beta)^{0.9187} \quad (45)$$

$$HTPI = 3.6813\ Re_{sh}^{-0.0612}\ Pr_{sh}^{-0.1707}\ (1+\varphi)^{11.247}\ (1+\beta)^{0.8777} \quad (46)$$

Eqs. (44-46) are applicable for applying baffles configuration has a cut ratio of $\delta = 16.5\%$ and pitch ratio of $\lambda = 1.47$. Furthermore, the shell-side Reynolds and Prandtl values range from 3710 to 14580 and 3.13 to 6.9, respectively. Figs. 12 & 13 show comparisons of the experimental values of $\overline{\mathrm{Nu}}_{\mathrm{sh}}$, f_{sh}, and HTPI with those predicted by the correlations. From Fig. 12, it is recorded that for the exchangers without baffles (Eqs. (41-43)), all data are predicted using the suggested equations with maximum deviations of ±5.3%, ±5.9%, and ±7.1% for $\overline{\mathrm{Nu}}_{\mathrm{sh}}$, f_{sh}, and HTPI, respectively. While for the exchangers engaged with single segmental baffles (Eqs. (44-46)), Fig. 13 shows that all values are predicted with maximum deviations of ±7.0%, ±4.7%, and ±10.9% for $\overline{\mathrm{Nu}}_{\mathrm{sh}}$, f_{sh}, and HTPI, respectively.

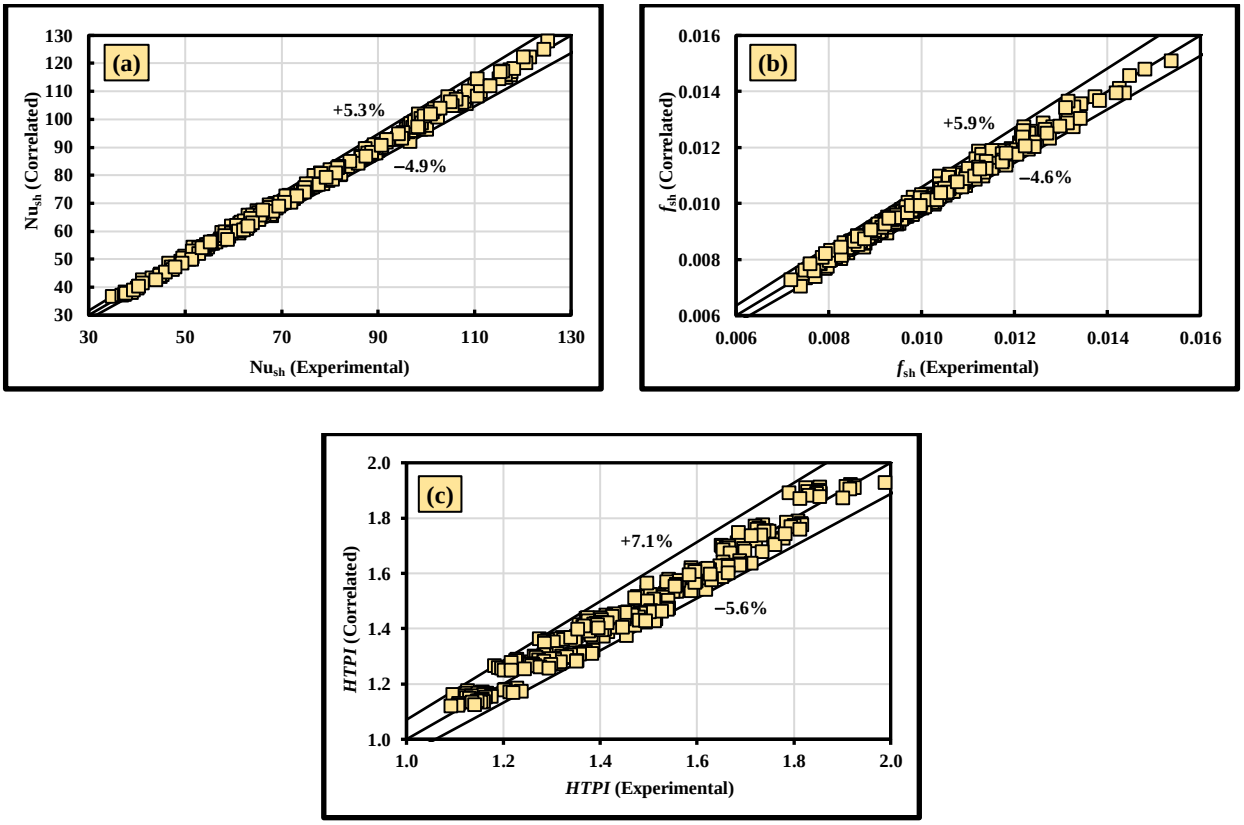

Fig. 12: Comparisons of the experimental values with that correlated by Eqs. (41-43); (a) $\overline{Nu}_{sh}$, (b) f_{sh}, (c) $HTPI$.

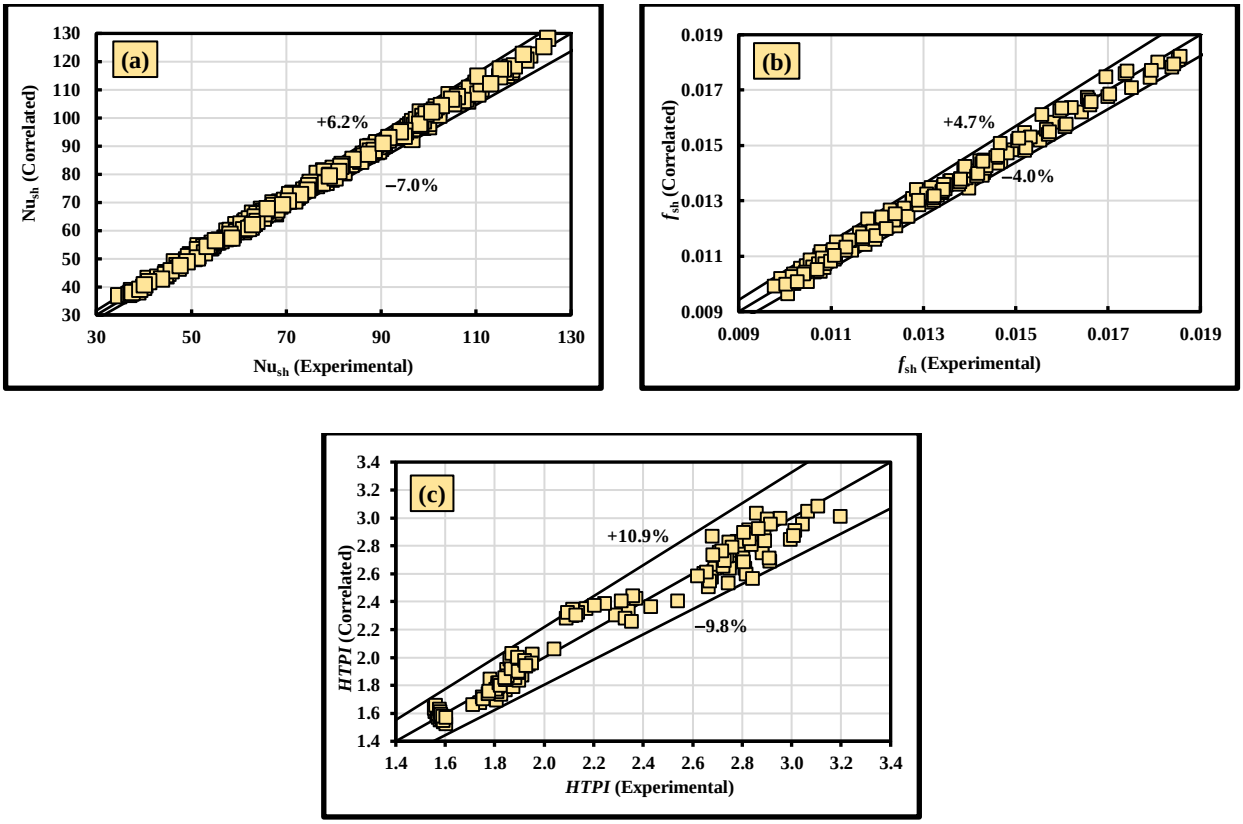

Fig. 13: Comparisons of the experimental values with that correlated by Eqs. (44-46); (a) $\overline{Nu}_{sh}$, (b) f_{sh}, (c) $HTPI$.

10 Conclusions

This study presents an experimental investigation of the hydrothermal attributes of a shell-tube heat exchanger of a counter flow configuration, which includes CCTs or SCTs of different base spacing ratios ($23.6\% \leq \beta \leq 55.1\%$). The experiments also cover the flow of cooling water or γ-Al_2O_3/water nanofluid loaded with different nanoparticle concentrations ($0 \leq \varphi \leq 1.5\%$) on the shell side. The experiments are accomplished for two cases: without or with single segmental baffles of fixed cut ratio of $\delta = 16.5\%$ and pitch ratio of $\lambda = 1.47$. A total of 432 tests are carried out on 6 heat exchangers for a variety of Reynolds numbers ($3550 \leq Re_{sh} \leq 14580$) and Prandtl numbers ($3.13 \leq Pr_{sh} \leq 7.28$). The results may be summarized as follows, based on the prior chapters and the data supplied by the experimental tests:

- Both the $\overline{Nu}_{sh}$ and f_{sh} of nanofluids are greater than the base fluid's at the same flow condition, and their increase grows as φ increases.
- The $\overline{Nu}_{sh}$ and f_{sh} are higher when incorporating SCTs instead of CCTs, and their increases grow with increasing the SCT spacing ratio. Compared with employing CCTs, the average increases in the $\overline{Nu}_{sh}$ and f_{sh} are 80.5% and 19.5%, respectively, at $\beta = 55.1\%$.
- The increases in $\overline{Nu}_{sh}$ and f_{sh} by the inclusion of γ-Al_2O_3 nanoparticles in the cooling water on the shell side have a greater influence on the increases with SCTs than CCTs.
- The $\overline{Nu}_{sh}$ is augmented as Re_{sh} increases and $T_{sh,i}$ decreases, while the $T_{sh,i}$ has a negligible impact on f_{sh}. Besides, f_{sh} is reduced by increasing Re_{sh}.
- Increasing the γ-Al_2O_3 nanoparticle concentration and the SCT base spacing ratio, besides reducing the shell-side flow rate and inlet temperature, augments the HTPI.
- The maximum obtained HTPI is 3.19, obtained by utilizing baffles of $\delta = 16.5\%$, $\lambda = 1.47$, γ-Al_2O_3/water nanofluid of nanoparticle concentration of $\varphi = 1.5$, and SCTs of $\beta = 55.1\%$, and applying the lowest shell-side flow rate and inlet temperature.
- A series of correlations is provided to predict the average Nusselt number and Fanning friction factor of the shell side, as well as the HTPI of the tested heat exchangers.

References

[1] M.A. Mehrabian and M. Hemmat, "The Overall Heat Transfer Characteristics of a Double Pipe Heat Exchanger: Comparison of Experimental Data with Predictions of Standard", Transactions on Modelling and Simulation, vol. 30, 12 pages, 2001.

[2] A. Bejan and A.D. Kraus, "Heat Transfer Handbook", John Wiley & Sons, p. 1030, 2003.

[3] J. Wajs, M. Bajor, M. Bajor and D. Mikielewicz, "Thermal-Hydraulic Studies on the Shell-and-Tube Heat Exchanger with Minijets", Energies, vol. 12(17), Article ID 3276, 2019.

[4] B. Wang, J.J. Klemeš, N. Li, M. Zeng, P.S. Varbanov, Y. Liang, "Heat Exchanger Network Retrofit with Heat Exchanger and Material Type Selection: A review and a Novel Method", Renewable and Sustainable Energy Reviews, vol. 138, Article ID 110479, 2021.

[5] A. Dewan, P. Mahanta, K.S. Raju and P.S. Kumar, "Review of Passive Heat Transfer Augmentation Techniques", Proceedings of the Institution of Mechanical Engineers, Part A: Journal of Power and Energy, vol. 218, Part A: J. Power and Energy, A04804 © IMechE 2004.

[6] A.B. Ganorkar and V.M. Kriplani, "Review of Heat Transfer Enhancement in Different Types of Extended Surfaces", International Journal of Engineering Science and Technology (IJEST), vol. 3(4), pp. 3304–3313, April 2011.

[7] A.N. Mahureand and V.M. Kriplani, "Review of Heat Transfer Enhancement Techniques", International Journal of Engineering Research and Technology, vol. 5(3), pp. 241–249, 2012.

[8] M.R. Salem, R.K. Ali, R.Y. Sakr and K.M. Elshazly, "Experimental Study on Convective Heat Transfer and Pressure Drop of Water-Based Nanofluid Inside Shell and Coil Heat Exchanger", PhD thesis, Faculty of Engineering at Shoubra, Benha University, 2014.

[9] MR Salem, MN Owyed, RK Ali, "Experimental Investigation of the Performance Attributes of a Thermal Energy Storage Unit using Different System Configurations", Applied Thermal Engineering, vol. 230, Article ID 120678, 2023.

[10] M.R. Salem, M.K. Althafeeri, K.M. Elshazly, M.G. Higazy, M.F. Abdrabbo, "Experimental Investigation on the Thermal Performance of a Double Pipe Heat Exchanger with Segmental Perforated Baffles", International Journal of Thermal Sciences, vol. 122, pp. 39-52, 2017.

[11] A.B. Colaço, F. Bernardo, M.B. Lopes, V.C. Mariani, L.S. Coelho, M.R. Salem, "Optimization of Double Pipe-Heat Exchanger with Single Segmental Perforated Baffles", 17th Brazilian Congress of Thermal Sciences and Engineering November 25th-28th, 2018, Águas de Lindóia, SP, Brazil.

[12] A. Colaço, V.C. Mariani, M.R. Salem, L. dos Santos Coelho, "Maximizing the thermal performance index applying evolutionary multi-objective optimization approaches for double pipe heat exchanger", Applied Thermal Engineering, vol. 211, No. 118504, 2020.

[13] S.U. Choi and J.A. Eastman, "Enhancing Thermal Conductivity of Fluid with Nanoparticles", ASME International Mechanical Engineering Congress & Exposition, San Francisco, November 12-17, 1995.

[14] Q. Li and Y. Xuan, "Convective Heat Transfer and Flow Characteristics of Cu–Water Nanofluid", Science in China Series E: Technological Science, vol. 45(4), pp. 408–416, August 2002.

[15] S.K. Das, S.U. Choi, W. Yu and T. Pradeep, "Nanofluids: Science and Technology", John Wiley & Sons, Inc., Hoboken, New Jersey, 2007.

[16] S.U. Choi, Z.G. Zhang, W. Yu, F.E. Lockwood and E.A. Grulke, "Anomalously Thermal Conductivity Enhancement in Nanotube Suspension", Applied Physics Letters. vol. 79, pp. 2252–2254, 2001.

[17] X. Wang, S.U.S. Choi and X. Xu, "Thermal Conductivity of Nanoparticle-Fluid Mixture", Journal of Thermophysics and Heat Transfer, vol. 13(4), pp. 474–480, 1999.

[18] S. Lee, S.U. Choi, S. Li and J.A. Eastman, "Measuring Thermal Conductivity of Fluids Containing Oxide Nanoparticles", Journal of Heat Transfer, vol. 121, pp. 280–289, 1999.

[19] P. Keblinski, S.R. Phillpot, U.S. Choi and J.A. Eastman, "Mechanisms of Heat Flow in Suspensions of Nano-Sized Particles (Nanofluids)", International Journal of Heat and Mass Transfer, vol. 45, pp. 855–863, 2002.

[20] W. Yu and S.U. Choi, "The role of Interfacial Layers in the Enhanced Thermal Conductivity of Nanofluids: A Renovated Maxwell Model", Journal of Nanoparticle Research, vol. 5, pp. 167–171, 2003.

[21] S.M. Elshamy, M.T. Abdelghany, M.R. Salem, O.E. Abdellatif, "Energy and Exergy Analysis of Shell and Coil Heat Exchanger using Water Based Al2O3 Nanofluid Including Diverse Coil Geometries: An experimental Study", Journal of Nanofluids, vol. 9 (1), pp. 13-23, 2020.

[22] M.L. Magalhães, A.S. Pereira and S.J. Cartaxo, "Development of a Transient Model for Evaluation of Shell and Tube Heat Exchanger with Helical Baffles Applied for SiO2 Nanofluid", Journal of Advanced Thermal Science Research, vol. 5, pp. 9-16, 2018.

[23] M. Jahangiri, R.Y. Farsani, A.A. Shamsabadi, "Numerical Investigation of the Water/Alumina Nanofluid Within a Microchannel with Baffles", Journal of Mechanical Engineering and Technology, vol. 1(2), 67-76, 2018.

[24] Y. Khetib, H.M. Abo-Dief, A.K. Alanazi, S.M. Sajadi, S. Bhattacharyya and M. Sharifpur, "Optimization of Heat Transfer in Shell-and-Tube Heat Exchangers using MOGA Algorithm: Adding Nanofluid and Changing the Tube Arrangement", Chemical Engineering Communications, vol. 210(6), pp. 893-907, 2021.

[25] M. Bahiraei, M. Naseri, A. Monavari, "A Second Law Analysis on Flow of a Nanofluid in a Shell-and-Tube Heat Exchanger Equipped with New Unilateral Ladder Type Helical Baffles", Powder Technology, vol. 394, pp. 234-249, 2021.

[26] M.A. Alazwari and M.R. Safaei, "Combination Effect of Baffle Arrangement and Hybrid Nanofluid on Thermal Performance of a Shell and Tube Heat Exchanger Using 3-D Homogeneous Mixture Model", Mathematics, vol. 9(8), Article No. 881, 2021.

[27] F. Sharifat, A. Marchitto, M.S. Solari and D. Toghraie, "Analysis, Prediction, and Optimization of Heat Transfer Coefficient and Friction Factor of Water-Al2O3 Nanofluid Flow in Shell-and-Tube Heat Exchanger with Helical Baffles (using RSM)", The European Physical Journal Plus, vol. 137, Article ID 991, 2022.

[28] R.A. Silva, "Shell and Tube Heat Exchanger with Helical Baffles and Graphene Nanofluid: a CFD Analysis of its Performance and Characteristics. Mestrado em Engenharia Mecânica, Universidade Federal de Pernambuco, Recife, 2022.

[29] R. Gugulothu and N. Sanke, "Effect of Helical Baffles and Water-Based Al2O3, CuO, and SiO2 Nanoparticles in the Enhancement of Thermal Performance for shell and tube heat exchanger", Heat Transfer, vol. 51, pp. 3768–3793, 2022.

[30] L. Yang, S. Baghaei, W. Suksatan, P. Barnoon, S. sharma, A. Davidyants and A.S. El-Shafay, "Numerical Assessment of the Influence of Helical Baffle on the Hydrothermal Aspects of Nanofluid Turbulent Forced Convection inside a Heat Exchanger", Scientific Reports, vol. 12, Article ID 2245, 2022.

[31] S. Akcay and U. Akdag, "Effect of Baffle Angles on Flow and Heat Transfer in a Circular Duct with Nanofluids", International Advanced Researches and Engineering Journal, vol. 6(3), pp. 176–185, 2022.

[32] B. Souayeh, S. Bhattacharyya, N. Hdhiri, F. Hammami, E. Yasin, S.S. Raju, M.W. Alam, T. Alsheddi and M. Al Nuwairan, "Effect of Magnetic Baffles and Magnetic Nanofluid on Thermo-Hydraulic Characteristics of Dimple Mini Channel for Thermal Energy Applications", Sustainability, vol. 14, Article ID 10419, 2022.

[33] S. Rana, H.B. Dura, S. Bhattrai, R. Shrestha, "Impact of Baffle on Forced Convection Heat Transfer of CuO/Water Nanofluid in a Micro-Scale Backward Facing Step Channel", Journal of Thermal Engineering, vol. 8(3), pp. 310–322, 2022.

[34] M. Bouselsal, F. Mebarek-Oudina, N. Biswas and A.I. Ismail, "Heat Transfer Enhancement Using Al2O3-MWCNT Hybrid-Nanofluid inside a Tube/Shell Heat Exchanger with Different Tube Shapes", Micromachines. vol. 14(5), Article ID 1072, 2023.

[35] M.R. Salem, Experimental Investigation on the Hydrothermal Attributes of MWCNT/Water Nanofluid in the Shell-Side of Shell and Semi-Circular Tubes Heat Exchanger", Applied Thermal Engineering, vol. 176, Article ID 115438, 2020.

[36] M. Moawed, "Thermal Performance of a Cross Flow Heat Exchanger with Semi-Circular Tubes", ERJ Shoubra Faculty of Engineering, vol. 4, pp. 87–109, June 2005.

[37] S.A. Nada, H. El-Batsh, M. Moawed, "Heat Transfer and Fluid Flow Around Semi-Circular Tube in Cross Flow at Different Orientations", Heat Mass Transfer, vol. 43, pp. 1157–1169, 2007.

[38] E.Z. Ibrahiem, A.O. Elsayed, "Heat Transfer Performance of a Semi-Circular Tube Bank", Heat Transfer Research, vol. 46(6), pp. 563–576, 2015.

[39] J.C. Maxwell, "Treatise on Electricity and Magnetism", 1st ed., Clarendon Press, Oxford, UK, 1873.

[40] J. Koo and C. Kleinstreuer, "Laminar Nanofluid Flow in Microheat-Sinks", International Journal of Heat and Mass Transfer, vol. 48, pp. 2652–2661, 2005.

[41] H.C. Brinkman, "The viscosity of Concentrated Suspensions and Solution", The Journal of Chemical Physics, vol. 20(4), pp. 571–581, 1952.

[42] C.J. Ho, W.K. Liu, Y.S. Chang and C.C. Lin, "Natural Convection Heat Transfer of Alumina–Water Nanofluid in Vertical Square Enclosures: An Experimental Study", International Journal of Thermal Sciences, vol. 49, pp. 1345–1353, 2010.

[43] Y. Xuan and W. Roetzel, "Conceptions for Heat Transfer Correlation of Nanofluids", International Journal of Heat and Mass Transfer, vol. 43, pp. 3701–3707, 2000.

[44] S.J. Kline and F.A. McClintock, "Describing Uncertainties in Single-Sample Experiments", Mechanical Engineering, vol. 75(1), pp. 3–8, January 1953.

[45] V. Gnielinski, "New Equations for Heat and Mass Transfer in Turbulent Pipe and Channel Flow", International Chemical Engineering, vol. 16, pp. 359–368, 1976.

[46] G.K. Filonenko, "Hydraulic Resistance of Pipes (Hydraulischer Widerstand von Rohrleitungen)," Teploenergetika, vol. 1(4), pp. 40–44, 1954.

[47] M.R. Salem, M. Eltoukhey, R. Ali, K. Elshazly, "Experimental Investigation on the Hydrothermal Performance of a Double-Pipe Heat Exchanger using Helical Tape Insert", International Journal of Thermal Sciences, vol. 124, pp. 496–507, 2018.

[48] H.H. Al-Kayiem, A. Bin Ekhwan, L.N. Muhi, "Augmentation of Ribs Turbulators Height on the Hydrothermal Performance of Double Pipe Heat Exchanger", Journal of Engineering Science and Technology, vol. 12(2), pp. 548-563, 2017.

Nomenclatures

A	Area, m^2
Cp	Specific heat at constant pressure, $J/kg.℃$
d	Diameter, m
f	Fanning friction factor
h	Convection heat transfer coefficient, $W/m^2.℃$
k	Thermal conductivity, $W/m.℃$
L	Length, m
m	Mass, kg
$\dot{m}$	Mass flow rate, kg/s
N	Number
P	Pressure, Pa
p	Pitch, m
Q	Heat transfer rate, W
S	Spacing, m
T	Temperature, ℃
U	Overall heat transfer coefficient, $W/m^2.℃$
u	Velocity, m/s
V	Volume, m^3
$\dot{V}$	Volume flow rate, m^3/s

Dimensionless groups

$\overline{Nu}$	Average Nusselt number
Pr	Prandtl number
Re	Reynolds number
St	Stanton number

Greek letters

β	Base spacing ratio
δ	Baffles cut ratio
Δ	Differential
Φ	Volume concentration
γ	Gamma type of alumina
K	Boltzmann constant $\cong 1.3807 * 10^{-23}$ J/K
Γ	Modelling function is incorporated in Eqs. (9) & (14)
λ	Baffles pitch ratios
ω	Uncertainty
μ	Dynamic viscosity, $kg/m.s$
π	Pi ≡ A mathematical constant ≅ 3.1416
ρ	Density, kg/m^3
χ	Modelling function is incorporated in Eqs. (9) & (14)
ζ	Ratio of the nanolayer thickness to the original particle radius

Superscripts and subscripts

0	No modification
ave	Average
b	Base
bf	Base fluid
h	Hydraulic
i	Inner or inlet or internal
LM	Logarithmic Mean
m	Modified
nf	Nanofluid
np	Nanoparticles
o	Out or outer
sh	Shell
t	Tube

Acronyms and abbreviations

Al_2O_3	Alumina
CCT	Complete Circular Tube
CuO	Copper Oxide
HTPI	Hydrothermal Performance Index
MWCNT	Multiwalled Carbon Nanotubes
SCT	Semi-Circular Tube